

EXPERIMENTAL AND NUMERICAL STUDY OF FLAME CHARACTERISTICS OF H₂/LANDFILL GAS LAMINAR PREMIXED COMBUSTION

Ruicai YANG¹, Guangchao LIU¹, Fang WANG¹, Wenchao YANG², Guoyan CHEN² *

¹Department of Information Engineering, Henan College of Industry & Information Technology, Jiaozuo 454000, China

²School of Mechanical and Power Engineering, Henan Polytechnic University, Jiaozuo 454003, China

* Corresponding author; E-mail: 254568182@qq.com

This paper mainly conducts experimental and numerical simulation studies on the combustion characteristics of H₂/landfill gas laminar premixed flames. The laminar burning velocity of CH₄/CO₂/H₂ mixtures is measured with a fixed-volume combustion bomb. The study results indicate the mixture's laminar burning velocity approximately grows linearly with the H₂ content, and the rate of increase also rises with the increase of equivalence ratio. The variation trend of the adiabatic flame temperature with equivalence ratio is similar to that of laminar burning velocity. Compared to the thermal diffusivity, The adiabatic flame temperature has a greater effect on laminar burning velocity. Under lean combustion conditions, as the H₂ content increases, the thermal diffusion instability gradually intensifies, while it is the opposite under rich combustion conditions. The hydrodynamic instability gradually intensifies with the increase of H₂ content, while first intensifies and then weakens with the increase of equivalence ratio. The increase in H₂ content enhances the laminar burning velocity by increasing the mole fraction of relevant free radicals and the reaction rate of the main reaction. The maximum mole fraction of NO gradually increases with the rise of the H₂ content for different equivalence ratios. The increase in H₂ content strengthens the contribution of thermal mechanism reactions in NO formation.

Key words: H₂/landfill gas premixed flame; Laminar burning velocity; Flame instability; NO emission

1. Introduction

Nowadays, the consumption of fossil fuels and impact of air pollution on the human living environment have become increasingly severe. Therefore, finding a clean energy alternative to fossil fuels is of critical importance for China's energy transition and ecological environmental protection [1, 2]. Landfill gas consists of a mixture of gases with combustible components produced by the decomposition of solid waste in landfills by microorganisms. Its primary components are CH₄ and CO₂, with small amounts of air and other impurities [3, 4]. Studies have shown that CO₂ can effectively radiate and absorb heat generated during combustion, significantly reducing the burning velocity [5-7]. This reduction, in turn, lowers flame temperature, combustion rate, and flame stability. As a result, the industrial application of landfill gas is significantly limited [8-10]. To improve the combustion

performance of landfill gas, it is commonly mixed with high-calorific-value fuels. H₂, due to its high calorific value and environmentally friendly combustion products, is the preferred choice for blending [11-14]. Therefore, studying the influence of adding H₂ on burning properties of landfill gas holds significant theoretical and practical value for its real-world applications.

The laminar burning velocity (S_L) is an important parameter in characterizing combustion properties. It's crucial for validating the reliability of chemical reaction mechanisms and for developing accurate premixed flame combustion models [15, 16]. The source and production process of biogas are slightly different from landfill gas, but their compositions are similar, with CH₄ and CO₂ being the main component. Zhen *et al.* [17] used the Bunsen burner method to study stability and heat release properties of premixed biogas-H₂-air flames. Their research found that as H₂ content increased, the S_L of the biogas-air mixture increased monotonically. Wei *et al.* [18] conducted numerical studies on H₂-rich biogas-air one-dimensional laminar premixed flames with the simplified reaction kinetic mechanism GRI 3.0. They found that because of joint impact of thermal, dilution, and chemical effects, CO₂ reduced heat release rate of the biogas-air mixture, while adding H₂ significantly increased the heat release rate. Benaissa *et al.* [19] investigated how adding H₂ influences the burning behavior of biogas-H₂-air premixed mixtures. This finding indicated H₂ addition to biogas enhanced the flame's S_L , cut down the combustion duration, and reduced the ignition delay time. Kahangamage *et al.* [20] carried out numerical analyses of the laminar combustion properties of H₂-rich, low heat value landfill gas. Their results showed that when equivalence ratio (Φ) falls between 0.7 and 1.4, S_L grew with higher H₂ contents and initial temperatures but decreased significantly with increased initial pressure. At high initial pressures, S_L was less sensitive to changes in the H₂ contents. Boussetla *et al.* [21] studied deeply NO emission from MILD combustion of the mixture biogas-syngas, five NO routes are considered, specifically: thermal, prompt, NNH, N₂O and reburning, they found that temperature grows up rapidly and the MILD regime disappears when O₂ increases in oxidizer, in addition, O₂ increasing in the oxidizer improves thermal mechanism which surpasses prompt one at 17% of O₂ volume and governs NO production.

Existing research indicates that studies on the combustion characteristics of H₂/landfill gas premixed flame are limited, particularly regarding its flame instability and NO emission characteristics. Therefore, this study, building on previous research, focuses on exploring the effects of variations in H₂ content and Φ on the flame instability. Additionally, the mechanism of S_L variation is revealed by sensitivity analysis and changes in chemical reaction rates, and the NO emission is deeply investigated through the mole fraction and rate of production, aiming to provide a theoretical basis for improving the combustion performance of landfill gas and for its future use as an energy resource.

2. Experimental methods and numerical simulation

2.1. Experimental methods

In this study, the experimental setup primarily consists of several key components, including a Schlieren system, ignition system, constant-volume combustion chamber, data acquisition system, and high-speed camera system [22, 23]. A Schematic diagram of the experimental system is shown in Fig. 1. The combustion chamber has internal dimensions measuring 200 mm by 200 mm, resulting in a total volume of 6.3 L. Transparent glass windows, the diameter measures 170 mm, are installed on combustion chamber for observation of flame propagation process. The ignition system uses a high-energy pulse igniter to ignite two 0.45 mm tungsten wires symmetrically positioned at the center of the

combustion chamber. A pressure sensor is used to monitor pressure changes inside combustion chamber in real-time, with a sampling frequency of 200 kHz and an accuracy of 0.25% FS. To ensure the reproducibility of the experimental results, each experiment was repeated at least three times under the same initial conditions. The uncertainty analysis of the S_L measurement is presented at the end of Section 2.2.

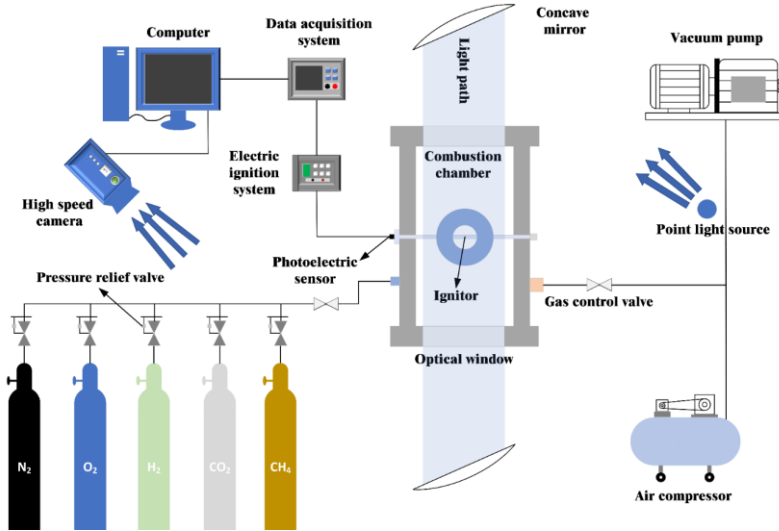


Fig. 1. Schematic diagram of experimental system

Table 1. Comprehensive fuel mixture chart

Number	Fuel components (%)			X_{H_2} (%)	Density(kg/m ³)
	CH ₄	CO ₂	H ₂		
F1		27	18	18	1.125
F2		22.5	22.5	22.5	1.114
F3	55	18	27	27	1.104
F4		13.5	31.5	31.5	1.094
F5		9	36	36	1.084

The specific composition of the mixed fuels which is used in the experimental study is provided in Tab. 1. The purity of the gas used in the experiment reached more than 99.99 %. The mixed fuels consist of 55% CH₄ by volume and a total of 45% by volume of H₂ and CO₂. According to the varying H₂ content, the mixtures are denoted as F1, F2, F3, F4, and F5, respectively.

The definition of the hydrogen content X_{H_2} is

$$X_{H_2} = \frac{V_{H_2}}{V_{CH_4} + V_{CO_2} + V_{H_2}} \quad (1)$$

Where, V_{CH_4} , V_{CO_2} , and V_{H_2} respectively represent the volume fractions of CH₄, CO₂ and H₂ in the mixed fuel.

$$\Phi = \frac{(A/F)_{stoic}}{A/F} \quad (2)$$

Where A/F is the actual air-to-fuel mass ratio in the gas mixture, and $(A/F)_{stoic}$ is the theoretical air-to-fuel mass ratio for complete combustion of the fuel under chemical equivalent conditions ($\Phi = 1$).

The initial temperature of the experiment is $T_0 = 300$ K and initial pressure is $P_0 = 1$ atm. The Φ is set between 0.8 and 1.2, with the initial mixture composed of CH_4 , CO_2 , and H_2 at a volume fraction ratio of 55:27:18. The H_2 volume fraction in the total fuel ranged from 18% to 36%.

2.2. Data processing

Figure 2 indicates the flame propagation images at different H_2 contents. The spherical flame in the combustion chamber is affected by the ignition energy during the initial propagation process. Therefore, the ignition energy is controlled below the maximum ignition limit of 6 J and the minimum effective flame radius is set to 10 mm to reduce the influence of the initial ignition energy on the experimental results [24]. Additionally, to reduce measurement uncertainty, the effective flame radius is kept under 0.3 times radius of the burning vessel [25]. Therefore, the range of effective flame radius is set between 10 mm and 30 mm. For the spherically propagating flame, Image-Pro Plus image analysis software is used in this study to process flame images to extract real-time flame radius r_f . The momentary variation in flame radius is subsequently employed to determine the stretched flame speed (S_b) and flame stretch rate (K). The expression for S_b is given by [26]:

$$S_b = \frac{dr_f}{dt} \quad (3)$$

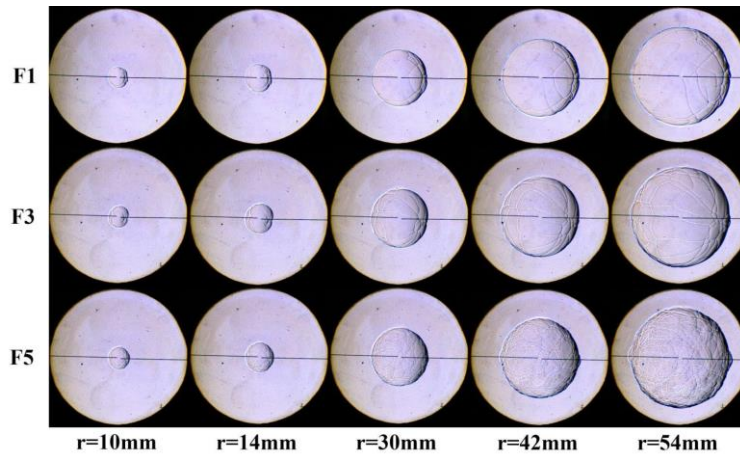


Fig. 2. Flame development images of F1, F3, and F5 captured by Schlieren ($\Phi = 1.0$, $P_0 = 1$ atm, $T_0 = 300$ K)

In the equation, r_f is the instantaneous radius of spherically expanding flame, and t represents time. The stretch rate K during spherical flame propagation process can be calculated by following equation [27]:

$$K = \frac{d(\ln A)}{dt} = \frac{1}{A} \frac{dA}{dt} = \frac{2}{r_f} \frac{dr_f}{dt} = \frac{2}{r_f} S_b \quad (4)$$

In the equation, A represents the area of the flame front. In the early phase of spherical flame propagation, when flame surface does not exhibit a significant cellular structure, an approximately linear relationship exists between stretched flame speed S_b and flame stretch rate K :

$$S_b = S_b^0 - L_b K \quad (5)$$

In the equation, S_b^0 represents the unstretched flame speed, and L_b represents Markstein length. Finally, determination of S_L is based on the principle of mass conservation in the reaction zone near flame front.

$$S_L = \frac{1}{\sigma} S_b^0 = \frac{\rho_b}{\rho_u} S_b^0 \quad (6)$$

In the equation, σ represents the expansion coefficient, where ρ_b and ρ_u represents the densities of the burned and unburned gas mixtures, individually.

Flame stability is an important indicator for evaluating the combustion properties of premixed laminar flames. It primarily includes thermal-diffusive instability, hydrodynamic instability, and buoyancy instability [28]. Buoyancy instability typically only has a profound effect on flame propagation when the laminar burning velocity is below 15 cm/s. Since the S_L under different conditions in this study all exceed this value, the effect of buoyancy instability is disregarded [29]. The impact of thermal-diffusive and hydrodynamic instabilities is examined through the calculation of the Lewis number (Le), thickness (δ) of laminar flame and thermal expansion ratio (σ).

The equation used to compute δ is presented below:

$$\delta = \frac{T_{ad} - T_0}{(dT/dx)_{max}} \quad (7)$$

In the equation, T_{ad} is the adiabatic flame temperature of the gas mixture, T_0 represents initial temperature, while $(dT/dx)_{max}$ represents the maximum value of temperature gradient.

Le serves as a crucial parameter that reflects the unequal rates of thermal and mass diffusion, and it's commonly used to analyze the extent of thermal-diffusive instability. Its calculation formula is as follows:

$$Le = \frac{\alpha}{D_{ij}} = \frac{\lambda}{\rho_u c_p D_{ij}} \quad (8)$$

In the equation, λ denotes thermal conductivity, c_p represents specific heat capacity at constant pressure, and α represents thermal diffusivity. D_{ij} refers to mass diffusion coefficient of deficient reactant with respect to N_2 . Equation (8) computes Le corresponding to a single-component fuel combustible mixture. However, for mixed reactant fuels with at least two combustible substances, the effective Lewis number Le_{eff} can assess the thermal-diffusive instability. In this study, volume-weighted method is used to calculate Le_{eff} as outlined below:

$$Le_{eff} = \sum_{i=1}^n x_i Le_i \quad (9)$$

x_i represents volume fraction of each component in the combustible mixture, and Le_i represents Lewis number of component i in the combustible mixture.

In this experiment, the measurement error of S_L primarily comes from computational errors and measurement inaccuracies. (1) The computational error primarily stems from inaccuracies in extracting the flame radius. Due to the use of a high-speed camera and a Schlieren system, the error in extracting the flame radius is deemed negligible. (2) Measurement errors primarily originate from the precision of the digital manometer and initial temperature and pressure conditions. The digital manometer error is maintained between 1% and 3%, while initial temperature and pressure deviations are confined to ± 3 K and ± 3 kPa, respectively. The error of the initial temperature is below 1%, and the error of the initial pressure is below 3%. The total experimental error is less than 5%.

2.3. Numerical simulation

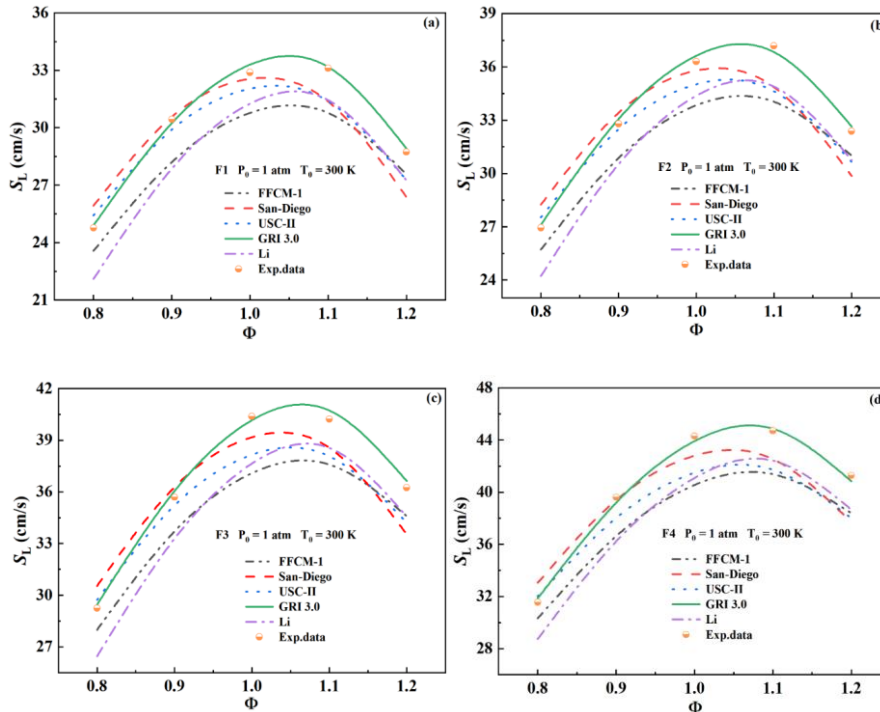
In the study, the laminar combustion characteristics of premixed flame are numerically simulated with the PREMIX module in CHEMKIN-Pro. The PREMIX is a FORTRAN program for modeling steady laminar one-dimensional premixed flames. Computational domain ranged from -2 cm to 10 cm,

GRAD and CURV are both assigned values of 0.02 to satisfy boundary conditions for free flame propagation and no thermal diffusion. A grid size of 900 is used to guarantee complete convergence of the flame speed and meet the required computational accuracy. T_{ad} is determined by chemical and phase equilibrium modules.

3. Results and analysis

3.1. Mechanism validation

To verify the reliability of the mechanisms, Fig 3 shows the S_L of $CH_4/CO_2/H_2$ mixtures with five different H_2 contents in the Φ range of 0.8 to 1.2, and the experimental data are compared with the predicted results from five commonly used mechanisms. Comprehensive details regarding these mechanisms are provided in Tab. 2. As shown in the figures, under lean combustion conditions, the prediction results for the mixture's S_L based on the USC-II and GRI 3.0 mechanisms fit well with experimental results for F1, F2, and F3 conditions. However, at $\Phi = 0.9$ under F4 and F5 conditions, the USC-II mechanism underpredicts, while the predictions of the GRI 3.0 and San-Diego mechanisms are more accurate. At $\Phi = 1.0$, under F1 and F2 conditions, the predictions from the GRI 3.0 and San-Diego mechanisms are more accurate. As the H_2 content increases further, the San-Diego mechanism underpredicts, while the GRI 3.0 mechanism still provides better predictions. Under rich combustion conditions, only the predictions from the GRI 3.0 mechanism fit well, while the predictions from the other four mechanisms are all lower than the experimental data. Overall, the GRI 3.0 mechanism provides the best prediction results. Therefore, GRI 3.0 mechanism is selected for subsequent simulation calculations.



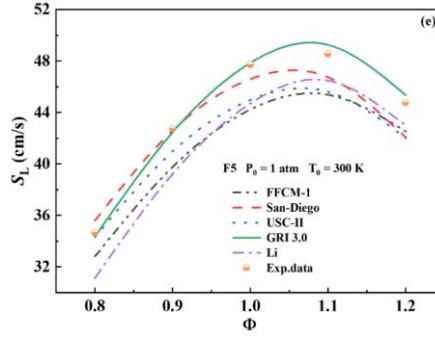


Fig. 3. Comparison of experimental and predicted Laminar burning velocity (S_L)

Table 2. Detailed information of the mechanisms

mechanism	species number	reaction number	reference
FFCM-1	38	291	[30]
San-Diego	57	268	[31]
USC-II	111	784	[32]
GRI 3.0	53	325	[33]
Li	21	102	[34]

3.2. Laminar burning velocity

Figure 4(a) illustrates the changes in S_L with Φ at different H_2 contents. The figure clearly demonstrates that as Φ increases, S_L grows at first and then diminishes, reaching its maximum value near $\Phi = 1.05$. Figure 4(b) depicts the relationship between S_L and the H_2 contents. As H_2 content increases, S_L increases approximately linearly, and the rate of increase rises as the Φ increases. From F1 to F5 and Φ rises from 0.8 to 1.2, the S_L of the mixture increased by 9.5 cm/s, 12.3 cm/s, 14.5 cm/s, 16.1 cm/s, and 16.5 cm/s, individually, with corresponding growth rates of 27.6%, 28.8%, 30.4%, 32.6%, and 36.2%. This phenomenon may be due to different factors influencing the change in S_L . Under lean combustion conditions, the excess oxidizer is inert in the combustion process and serves as a diluent, at this point, thermal effect plays a crucial role in influencing S_L , so addition of H_2 has minimal impact on improving S_L . However, under rich combustion conditions, the combustion reaction of the mixture is more complete, and the enhancement of chemical effects caused by H_2 addition increased S_L .

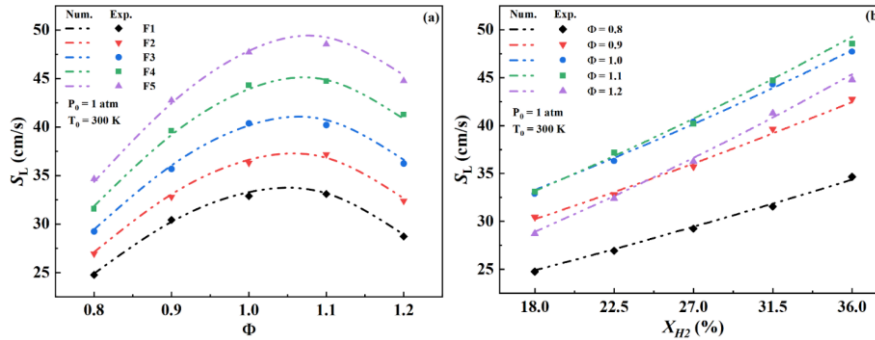


Fig. 4. The Laminar burning velocity (S_L) at different Φ and H_2 contents

3.3. Adiabatic flame temperature and thermal diffusivity

S_L is generally positively correlated with adiabatic flame temperature (T_{ad}) and thermal diffusivity (α) of the mixture. A higher T_{ad} increases the reaction rate constant, making the combustion reaction more intense and accelerating the combustion process. A higher thermal diffusivity allows heat released by the combustion reaction to be transferred more quickly to the unburned zone, promoting the occurrence of chemical reactions [35, 36]. Figure 5 illustrates the changes in T_{ad} and α with Φ at different H_2 contents. As depicted in Fig. 5(a), as Φ grows, T_{ad} of the mixture first increases and then decreases, attaining its highest value at $\Phi = 1.0$. Furthermore, as the H_2 content increases, the T_{ad} has increased for different Φ . As illustrated in Fig. 5(b), α rises as Φ increases, moreover, its rate of increase slightly rises as H_2 content increases. α significantly increases with the increase of H_2 content. However, the trend of T_{ad} 's variation with Φ is consistent with that of S_L , which indicates that compared with α , T_{ad} has a greater impact on S_L . Furthermore, from previous analysis for Fig. 4, it is evident that the S_L of the mixture attains its highest value near $\Phi = 1.05$, while the peak value of T_{ad} occurs at $\Phi = 1.0$. This indicates a slight shift in the Φ corresponding to the peak S_L relative to T_{ad} , this can be attributed to the combined influence of T_{ad} and α .

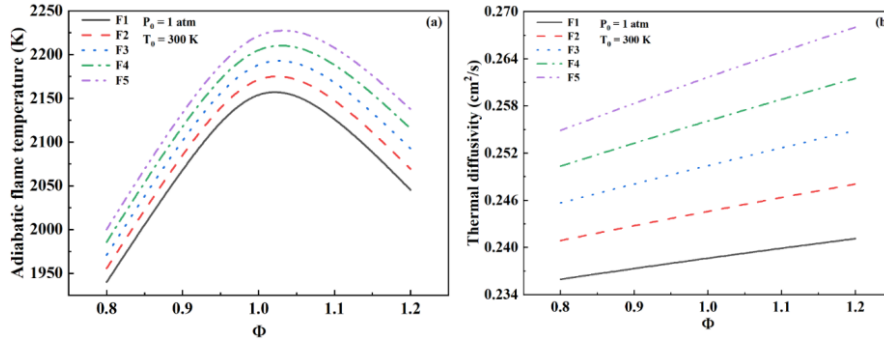


Fig. 5. Adiabatic flame temperature and thermal diffusivity at different Φ and H_2 contents

3.4. Analysis of laminar premixed flame instability

During combustion, the gas mixture undergoes thermal diffusion and mass diffusion. Thermal-diffusive instability mainly arises from unequal rates of thermal and mass diffusion at the flame front, causing irregular wrinkles and cellular structures on the flame surface. Typically, thermal-diffusive instability can be characterized by the effective Lewis number. The heat generated during the combustion of the mixture causes temperature changes in the unburned and burned gases around the flame. Due to the thermal expansion and contraction properties of gases, density differences arise, leading to flame instability, a phenomenon known as hydrodynamic instability. Thermal expansion ratio (σ) and flame thickness (δ) are key indicators that define hydrodynamic instability. Figure 6 illustrates the changes in Le_{eff} , σ and δ with Φ at different H_2 contents. Figure 6(a) shows that as Φ increases, the Le_{eff} of the mixtures at different H_2 contents gradually increase, indicating that the thermal diffusion instability of the flame gradually weakens. When $\Phi > 1$, the Le_{eff} of the mixtures is more than 1, indicating that thermal diffusion and mass diffusion of the flame tend to stabilize under rich combustion conditions. Furthermore, under lean combustion conditions, Le_{eff} decreases with the increase of H_2 content, while under rich combustion conditions, it increases with the increase of H_2 content. This

indicates that the thermal diffusion instability of the flame gradually increases with the increase of H₂ content under lean combustion, but the opposite is true under rich combustion.

From Fig. 6(b), it can be seen that as Φ rises, σ of mixture grows at first and then diminishes. The larger the σ , the greater the density ratio across the flame front, leading to more significant thermal expansion and more intense hydrodynamic instability. Therefore, as the Φ increases, hydrodynamic instability caused by σ first strengthens and then weakens. It is evident from Fig. 6(c) that as Φ increases, δ first decreases and then increases, attaining its highest value at $\Phi = 1.1$. Generally, the smaller the δ , the weaker tensile resistance of the flame, and the more intense hydrodynamic instability. Therefore, as Φ increases, hydrodynamic instability caused by δ first strengthens and then weakens. Furthermore, as can be seen from Fig. 6(b) and Fig. 6(c), under different Φ , with the increase of H₂ content, σ gradually increases and δ gradually decreases. This indicates that the hydrodynamic instability of the flame gradually intensifies with the increase of H₂ content.

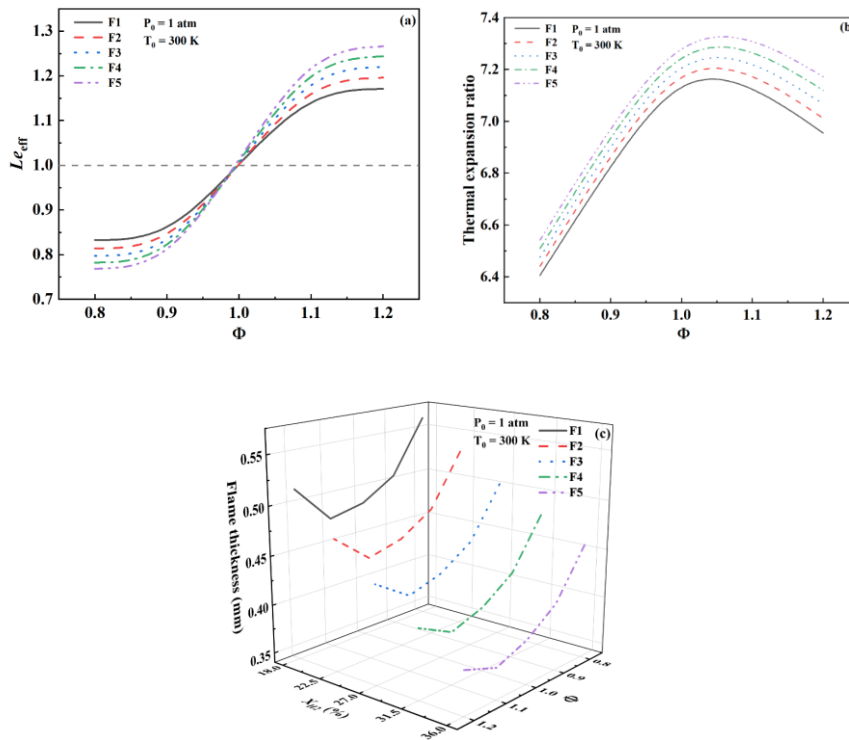


Fig. 6. The variations in effective Lewis number (Le_{eff}), thermal expansion ratio (σ) and flame thickness (δ)

3.5. Chemical kinetic analysis

To further investigate the influence of H₂ content on S_L , this study analyzed the key reactions during the combustion process of the mixture. Figure 7 shows the sensitivity coefficients of key reactions, mole fractions of important species and changes in net reaction rates at different H₂ contents when $\Phi = 1.0$. The magnitude of sensitivity coefficient indicates the impact of the reaction on S_L , with positive values indicating a promoting effect on S_L and negative values indicating an inhibiting effect.

As shown in Fig. 7(a), sensitivity coefficients of reactions R38, R119, R97, R284, R99, and R166 are positive, indicating that they generate O and OH radicals during combustion, promoting S_L . Among them, R38 exhibits the greatest positive sensitivity value, making it the dominant reaction during

combustion, producing a significant amount of O and OH radicals. R97, R119, and R284 are the main reactions that consume CH_3 radicals, with R119 and R284 being significant sources of OH and H radicals, respectively. R99 is the oxidation reaction of CO, which consumes OH radicals and produces H radicals. R166 is the reaction that consumes CO and H radicals. R52 and R35 have large negative sensitivity coefficients, they consume large amounts of H radicals and generate stable intermediates, which suppresses S_L . As depicted in Fig. 7(b), as the H_2 content grows, the competing effects of these main reactions mentioned above dramatically escalates the mole fraction of radical species, including H, O, and OH [37], thereby promoting the combustion reactions and leading to an increase in S_L .

Figure 7(c) and Fig. 7(d) illustrates changes in net reaction rates of relevant reaction at F1 and F5. It is observed that the net reaction rates of main promote reactions R38 and R99 increase significantly from F1 to F5. the maximum net reaction rates of these two reactions individually increase by 68% and 47%. The net reaction rates of other promoting reactions, R97, R166, and R284, show slight increases, while reaction R119 shows no significant change. Meanwhile, the net reaction rates of main inhibitory reactions R52 and R53 also increase, while other inhibitory reactions, R35 and R45, show no significant change.

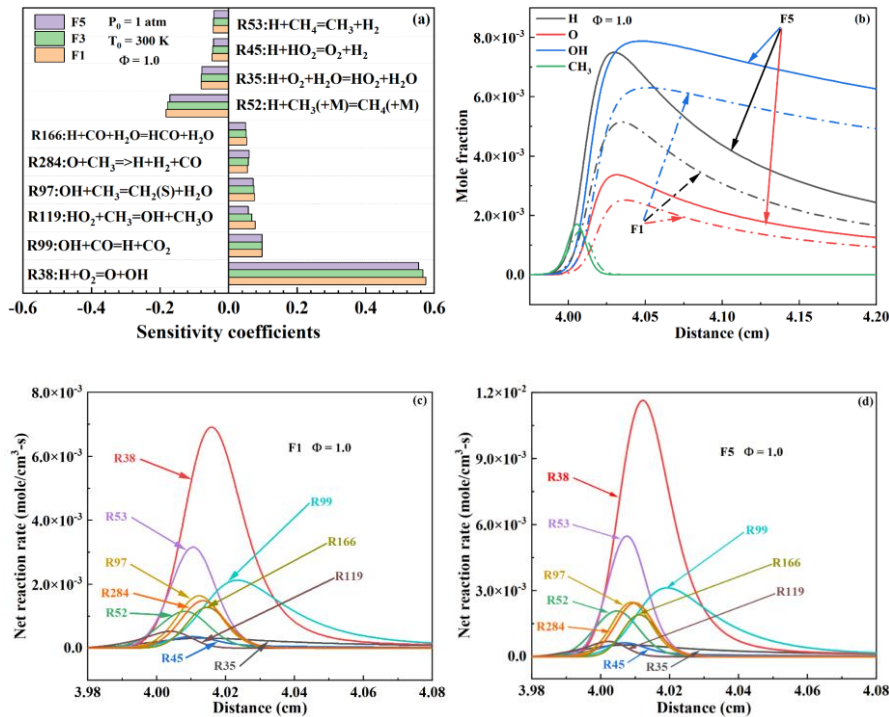


Fig. 7. Sensitivity analysis of key reactions, mole fractions of important species and changes in net reaction rates

3.6. Analysis of NO generation

During combustion, a large amount of NO is produced as heat release increases and flame temperature rises. This study conducts an in-depth analysis of the formation of NO under different H_2 content conditions by examining the mole fraction and rate of production. Figure 8(a) shows the variation of the maximum mole fraction of NO with the content of H_2 under different Φ . It is observed that the maximum mole fraction of NO gradually increases with the rise of the H_2 content for different

Φ . Furthermore, for the same H_2 content, as Φ increases, the maximum mole fraction of NO first increases and then decreases, and the peak of the maximum NO mole fraction occurs at $\Phi = 1.0$.

Figure 8(b) shows the variation of NO production rate with H_2 content under different Φ . It is observed that when the H_2 content is 0 and Φ is less than 1.1, the production rate of thermal NO increases with increasing Φ , but decreases when Φ exceeds 1.1. After adding H_2 , the thermal NO production rate continues to increase with increasing Φ for F3 and F5. However, the production rate of thermal NO for F1, as well as non-thermal NO for all H_2 contents, first increases with increasing Φ and then remains relatively unchanged. In addition, as H_2 content grows, the production rates of both thermal NO and non-thermal NO increase to varying degrees at different Φ . As the H_2 content increases from 0 to F5, the production rates of thermal NO and non-thermal NO increase by 204% and 170% at $\Phi = 0.9$, by 201% and 148% at $\Phi = 1.0$, and by 227% and 139% at $\Phi = 1.1$, respectively. This indicates that H_2 addition contributes more to the production of thermal NO. According to the previous analysis, adding H_2 increases the T_{ad} of the mixture, which could be the reason for the increased production of thermal NO.

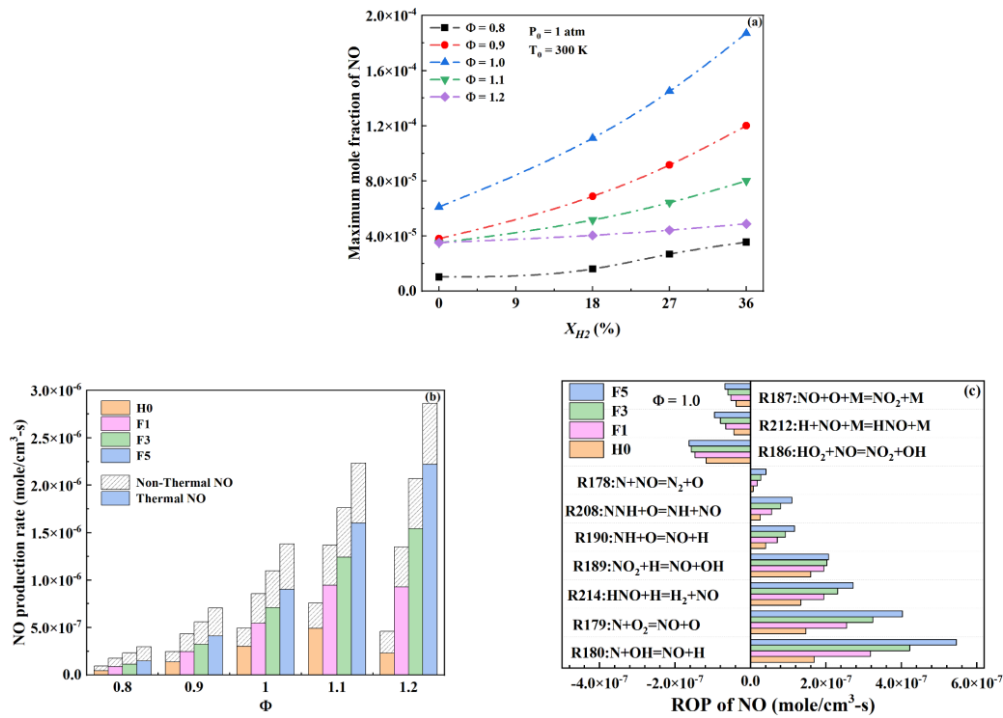


Fig. 8. Maximum mole fraction and production rate of NO

Figure 8(c) shows the variation of the rate of production (ROP) of the reaction related to NO with the content of H_2 when $\Phi = 1.0$. It is observed that the main reactions contributing to NO formation are R178, R179, R180, R189, R190, R208, and R214. As H_2 content grows, the ROP of these reactions increases to varying degrees. Compared to ROP of NNH mechanism NO reactions R208, R214, and R190, ROP of thermal mechanism NO reactions R179 and R180 increases more significantly with increasing H_2 contents. Thus, adding H_2 strengthens the contribution of thermal mechanism reaction to NO formation. Compared to NO formation reactions, the reaction rates of NO consumption reactions change less significantly. Therefore, the overall NO mole fraction grows as the H_2 content increases.

4. Conclusions

This paper mainly conducts experimental and numerical simulation studies on the combustion characteristics of H₂/landfill gas laminar premixed flames. It focuses on exploring the effects of variations in H₂ content and equivalence ratio (Φ) on the flame instability. Additionally, the mechanism of S_L variation is revealed by sensitivity analysis and changes in chemical reaction rates, and the NO emission is deeply investigated through the mole fraction and rate of production. The key conclusions of this research are as follows:

1. At different H₂ contents, the mixture's S_L grows at first and then diminishes as the Φ increases, reaching a peak near $\Phi = 1.05$. At the same Φ , S_L grows in an almost linear fashion with the growth of the H₂ content, and the rate of growth in S_L is greater at higher Φ .

2. The increase in H₂ content enhances T_{ad} and α , thereby promoting the improvement of S_L of the mixture. The peak equivalent ratios of T_{ad} and S_L are different, which can be attributed to the combined influence of T_{ad} and α . Moreover, the variation trend of T_{ad} with Φ is consistent with that of S_L , indicating that T_{ad} has a greater impact on S_L compared to α .

3. Under lean combustion conditions, as the H₂ content increases, the thermal diffusion instability gradually intensifies, while it is the opposite under rich combustion conditions. The hydrodynamic instability gradually intensifies with the increase of H₂ content, while first intensifies and then weakens with the increase of Φ .

4. With the rise of the H₂ content, the mole fractions of species including H, O, and OH increase significantly, and net reaction rates of main promote reactions R38 and R99 also increase substantially. The increase in S_L is the result of the competition of main reactions R38, R99, R52 and R35.

5. The maximum mole fraction of NO gradually increases with the rise of the H₂ content for different Φ . As the H₂ content increases, the ROP of main NO formation reactions increases. Compared to NNH mechanism NO reactions, the ROP of thermal mechanism NO reactions increase more significantly. The increase in H₂ content strengthens the contribution of thermal mechanism reactions in NO formation.

Acknowledgements

The authors appreciate the support of the Key Science and Technology Program of Henan Province, 252102240055; 252102240046. The authors appreciate the support of the Soft Science Research Program of Henan Provincial Key Scientific and Technological Projects, 252400411101.

References

- [1] Andeobu, L., *et al.*, Renewable hydrogen for the energy transition in Australia - Current trends, challenges and future directions, *International Journal of Hydrogen Energy*, 87 (2024), pp. 1207-1223
- [2] Chen, X. H., *et al.*, Assessing the environmental impacts of renewable energy sources: A case study on air pollution and carbon emissions in China, *Journal of Environmental Management*, 345 (2023), p. 118525
- [3] Parameswari, K., *et al.*, Sustainable landfill design for effective municipal solid waste management for resource and energy recovery, *Materials Today: Proceedings*, 47 (2021), pp. 2441-2449
- [4] Yaashikaa, P. R., *et al.*, A review on landfill system for municipal solid wastes: Insight into leachate,

- gas emissions, environmental and economic analysis, *Chemosphere*, 309 (2022), p. 136627
- [5] Khan, A. R., *et al.*, Investigation of dilution effect with N₂/CO₂ on laminar burning velocity of premixed methane/oxygen mixtures using freely expanding spherical flames, *Fuel*, 196 (2017), pp. 225-232
- [6] Xie, M., *et al.*, Numerical analysis on the effects of CO₂ dilution on the laminar burning velocity of premixed methane/air flame with elevated initial temperature and pressure, *Fuel*, 264 (2020), p. 116858
- [7] Zhang, W., *et al.*, Effect of diluent content and H₂/CO ratio on the laminar combustion characteristics of syngas, *International Journal of Hydrogen Energy*, 89 (2024), pp. 703-716
- [8] Lee, K., *et al.*, Generating efficiency and NO_x emissions of a gas engine generator fueled with a biogas–hydrogen blend and using an exhaust gas recirculation system, *International Journal of Hydrogen Energy*, 35 (2010), 11, pp. 5723-5730
- [9] Park, C., *et al.*, Performance and emission characteristics of a SI engine fueled by low calorific biogas blended with hydrogen, *International Journal of Hydrogen Energy*, 36 (2011), 16, pp. 10080-10088
- [10] Xin, Z., *et al.*, The experimental study on cyclic variation in a spark ignited engine fueled with biogas and hydrogen blends, *International Journal of Hydrogen Energy*, 38 (2013), 25, pp. 11164-11168
- [11] Li, J., *et al.*, Laminar burning Velocities, Markstein numbers and cellular instability of spherically propagation Ethane/Hydrogen/Air premixed flames at elevated pressures, *Fuel*, 364 (2024), p. 131078
- [12] Tang, C., *et al.*, Laminar burning velocities and combustion characteristics of propane–hydrogen–air premixed flames, *International Journal of Hydrogen Energy*, 33 (2008), 18, pp. 4906-4914
- [13] Tseng, C., Effects of hydrogen addition on methane combustion in a porous medium burner, *International Journal of Hydrogen Energy*, 27 (2002), 6, pp. 699-707
- [14] Wu, L., *et al.*, Experimental study on the effects of hydrogen addition on the emission and heat transfer characteristics of laminar methane diffusion flames with oxygen-enriched air, *International Journal of Hydrogen Energy*, 41 (2016), 3, pp. 2023-2036
- [15] Huang, Z., *et al.*, Measurements of laminar burning velocities for natural gas–hydrogen–air mixtures, *Combustion and Flame*, 146 (2006), 1, pp. 302-311
- [16] Wang, Q., *et al.*, Laminar combustion characteristics of methane/methanol/air mixtures: Experimental and kinetic investigations, *Case Studies in Thermal Engineering*, 41 (2023), p. 102593
- [17] Zhen, H. S., *et al.*, Characterization of biogas-hydrogen premixed flames using Bunsen burner, *International Journal of Hydrogen Energy*, 39 (2014), 25, pp. 13292-13299
- [18] Wei, Z. L., *et al.*, Effects of equivalence ratio, H₂ and CO₂ addition on the heat release characteristics of premixed laminar biogas-hydrogen flame, *International Journal of Hydrogen Energy*, 41 (2016), 15, pp. 6567-6580
- [19] Benaissa, S., *et al.*, Effect of hydrogen addition on the combustion characteristics of premixed biogas/hydrogen-air mixtures, *International Journal of Hydrogen Energy*, 46 (2021), 35, pp. 18661-18677
- [20] Kahangamage, U., *et al.*, Numerical investigation of combustion characteristics of hydrogen-enriched low calorific value landfill gas for energy applications, *Energy Reports*, 12 (2024), pp. 173-186
- [21] Boussetla, S., *et al.*, NO emission from non-premixed MILD combustion of biogas-syngas mixtures

- in opposed jet configuration, *International Journal of Hydrogen Energy*, 46 (2021), 75, pp. 37641-37655
- [22] Guo, S., *et al.*, Studies on the laminar burning properties of NH₃/H₂ blended fuel at different oxygen enrichment coefficient and hydrogen ratio, *International Journal of Hydrogen Energy*, 105 (2025), pp. 871-881
- [23] Hu, E., *et al.*, Experimental and numerical study on laminar burning characteristics of premixed methane–hydrogen–air flames, *International Journal of Hydrogen Energy*, 34 (2009), 11, pp. 4876-4888
- [24] Zhou, M., *et al.*, Effect of ignition energy on the uncertainty in the determination of laminar flame speed using outwardly propagating spherical flames, *Proceedings of the Combustion Institute*, 37 (2019), 2, pp. 1615-1622
- [25] Burke, M. P., *et al.*, Effect of cylindrical confinement on the determination of laminar flame speeds using outwardly propagating flames, *Combustion and Flame*, 156 (2009), 4, pp. 771-779
- [26] Davis, S. G., *et al.*, Markstein numbers in counterflow, methane- and propane- air flames: a computational study, *Combustion and Flame*, 130 (2002), 1, pp. 123-136
- [27] Li, H., *et al.*, Measurement of the laminar burning velocities and markstein lengths of lean and stoichiometric syngas premixed flames under various hydrogen fractions, *International Journal of Hydrogen Energy*, 39 (2014), 30, pp. 17371-17380
- [28] Lapalme, D., *et al.*, Characterization of thermodiffusive and hydrodynamic mechanisms on the cellular instability of syngas fuel blended with CH₄ or CO₂, *Combustion and Flame*, 193 (2018), pp. 481-490
- [29] Prathap, C., *et al.*, Investigation of nitrogen dilution effects on the laminar burning velocity and flame stability of syngas fuel at atmospheric condition, *Combustion and Flame*, 155 (2008), 1, pp. 145-160
- [30] G. P. Smith YTAH. Foundational Fuel Chemistry Model Version 1.0 (FFCM-1), <http://nanoenergy.stanford.edu/ffcm1.2016>
- [31] ***, Chemical-Kinetic Mechanisms for Combustion Applications, San Diego Mechanism web page, Mechanical and Aerospace Engineering (Combustion Research), University of California at San Diego (<http://combustion.ucsd.edu>)
- [32] Hai Wang X. USC Mech Version II. High-Temperature Combustion Reaction Model of H₂/CO/C1-C4 Compounds. http://ignis.usc.edu/USC_Mech_II.htm. 2007
- [33] Gregory. P. Smith, <http://combustion.berkeley.edu/gri-mech/>.
- [34] Li, J., *et al.*, A comprehensive kinetic mechanism for CO, CH₂O, and CH₃OH combustion, *International Journal of Chemical Kinetics*, 39 (2010), 3, pp. 109-136
- [35] Law, C. K., *Combustion Physics*, Cambridge University Press, 2010
- [36] Wen, L., *et al.*, Effect of oxygen enrichment and NH₃ pre-cracking on laminar burning velocity and intrinsic instability of NH₃/bio-syngas, *International Journal of Hydrogen Energy*, 94 (2024), pp. 485-496
- [37] Xiao, P., *et al.*, Experimental and kinetic investigation on the effects of hydrogen additive on laminar premixed methanol-air flames, *International Journal of Hydrogen Energy*, 44 (2019), 39, pp. 22263-22281

Submitted: 30.04.2025.

Revised: 13.06.2025.

Accepted: 16.06.2025.